Title: Investigating marine bio-calcification mechanisms in a changing ocean with *in vivo* and high-resolution *ex vivo* Raman spectroscopy

Running header: studying calcification via Raman spectroscopy

Authors and Affiliations: DeCarlo T.M.[1,2,3]*, Comeau S.[1,2,3#], Cornwall C.E.[1,2,3†], Gajdzik L.[4], Guagliardo P.[5] Sadekov A.[1,2,3], Thillainath E.C.[2,6], Trotter J.[2,7], and McCulloch M.T.[1,2,3]

[1]The University of Western Australia, Oceans Graduate School, 35 Stirling Highway, Crawley 6009, Western Australia, Australia

[2]Oceans Institute at The University of Western Australia, 35 Stirling Highway, Crawley 6009, Western Australia, Australia

[3]ARC Centre of Excellence for Coral Reef Studies, 35 Stirling Highway, Crawley 6009, Western Australia, Australia

[4]School of Molecular and Life Sciences, TrEnD Laboratory, Curtin University, Bentley 6102, Western Australia, Australia

[5]Centre for Microscopy, Characterisation and Analysis, The University of Western Australia, Crawley 6009, Western Australia, Australia

[6]The University of Western Australia, School of Biological Sciences, 35 Stirling Highway, Crawley 6009, Western Australia, Australia

[7]The University of Western Australia, School of Earth Sciences, 35 Stirling Highway, Crawley 6009, Western Australia, Australia

[#]Present address: Sorbonne Université, CNRS-INSU, Laboratoire d'Océanographie de Villefranche, 181 chemin du Lazaret, F–06230 Villefranche-sur-mer, France

[†]Present address: School of Biological Sciences, Victoria University of Wellington, Wellington, New-Zealand.

***Corresponding author:** thomas.decarlo@uwa.edu.au, +61409895484

Paper type: Technical Advance

Abstract

Ocean acidification poses a serious threat to marine calcifying organisms, yet experimental and field studies have found highly diverse responses among species and environments. Our understanding of the underlying drivers of differential responses to ocean acidification is currently limited by difficulties in directly observing and quantifying the mechanisms of bio-calcification. Here we present Raman spectroscopy techniques for quantifying the skeletal mineralogy and calcifying fluid chemistry of marine calcifying organisms such as corals, coralline algae, foraminifera, and fish (carbonate otoliths). First, our *in vivo* Raman technique is the ideal tool for investigating non-classical mineralization pathways. This includes calcification by amorphous particle attachment, which has recently been controversially suggested as a mechanism by which corals resist the negative effects of ocean acidification. Second, high-resolution *ex vivo* Raman mapping reveals complex banding structures in the mineralogy of marine calcifiers, and provides a tool to quantify calcification responses to environmental variability on various timescales from days to years. We describe the new insights into marine bio-calcification that our techniques have already uncovered, and we consider the wide range of questions regarding calcifier responses to global change that can now be proposed and addressed with these new Raman spectroscopy tools.

Main text

1. Introduction

The production of calcium carbonate ($CaCO_3$) by marine calcifying organisms plays a key role in the global carbon cycle and influences the chemistry of the ocean (Berelson et al., 2007). Biological calcification (or "bio-calcification") is performed by a variety of species in different environments that is manifested, for example, as the immense geologic reef structures built by corals and coralline algae, as well as being essential to calcareous plankton such as foraminifera and to the formation of calcium carbonate structures in the inner ears of fishes. The evolutionary history of bio-calcification extends back hundreds of millions of years and is found in multiple kingdoms, reflecting the many benefits that calcium carbonate mineralization provides, including skeletons for protection, structural support, and balance (Knoll, 2003). This widespread utility of calcification by marine organisms has depended on the favorability of calcium carbonate to form in seawater, with saturation states (Ω) of the calcium carbonate minerals aragonite and calcite exceeding one (*i.e.* oversaturation) in surface waters for hundreds of millions of years (Tyrrell & Zeebe, 2004; Zeebe, Ridgwell, & Zachos, 2016).

However, with humans now emitting CO_2 at rates that are likely unprecedented even on geologic timescales (Zeebe, Ridgwell, & Zachos, 2016), the carbonate chemistry of the surface oceans is fundamentally changing in ways that many calcifying taxa have not experienced in their evolutionary history (Hönisch et al., 2012; Tyrrell & Zeebe, 2004). Some previous mass extinctions of marine calcifying species have occurred under changes in ocean carbonate chemistry (especially with respect to Ω) that may have been less than the changes expected within the coming centuries due to the rapid release of CO_2 from human activities (Hönisch et al., 2012; Ridgwell & Schmidt, 2010; Veron, 2008). Therefore, although extant taxa may respond differently from those affected during previous mass extinctions, modern

CO_2-driven ocean acidification raises serious concerns about the future survival of calcifying species as well as the persistence of marine bio-calcification in general.

Forecasting the impacts of ocean acidification on marine calcifying organisms requires an understanding of the mechanisms by which they produce their calcium carbonate structures. It is clear that a range of calcification mechanisms exist because various organisms build their shells and skeletons with different calcium carbonate minerals. For example, aragonite is utilized by many corals and fishes, whereas calcite is utilized by most coralline algae and foraminifera. However, the classic notion that such organisms directly precipitate these different minerals has come under question. Recent studies have speculated that corals build their aragonitic skeletons from amorphous calcium carbonate (ACC) particles (Mass et al., 2017; Von Euw et al., 2017), that planktonic foraminifera form vaterite as a precursor to calcite (Jacob et al., 2017), and that some coralline algae stabilize their skeletons with dolomite and magnesite (Nash et al., 2013, 2011). These unexpected findings imply greater complexities in marine bio-calcification and underscore the need for further investigations into the mechanisms by which calcification occurs. Additionally, the response of various calcifiers to ocean acidification likely depends on their mineralogy due to the different solubilities of carbonate minerals (Morse, Mucci, & Millero, 1980).

We present Raman spectroscopy techniques for investigating the mineralogy of calcium carbonate structures in marine calcifying organisms with two complementary approaches: *in vivo* and high-resolution *ex vivo* mapping. Raman spectroscopy exploits the inelastic scattering of light to characterize sample mineralogy and the chemical bonding environment of crystals forming the shells and skeletons (E. Smith & Dent, 2005). Since Raman spectroscopy is highly sensitive to the various calcium carbonate minerals (Dandeu et al., 2006; Perrin et al., 2016; Stolarski et al., 2016), it is an ideal tool for investigating pre-cursor phases within calcified structures. Furthermore, Raman spectroscopy has recently been

applied to aragonitic corals to quantify the calcifying fluid aragonite saturation state (Ω_{Ar}) and its sensitivity to ocean acidification (DeCarlo et al., 2017). A key advantage of our *in vivo* approach presented here is the non-invasive nature of the technique, which removes the need for sample preparation or sacrificing the organism, two potential issues which could have confounded some previous results. We apply *in vivo* Raman spectroscopy to two species of aragonitic corals, a foraminifer, and a coralline alga. Additionally, we create high-resolution (micron-scale) *ex vivo* Raman maps of the calcium carbonate structures of a tropical coral, a deep-sea coral, a fish otolith, a foraminifer, and a coralline alga.

2. Materials and Methods

2.1 Sample collections

2.1.1 Specimens for *in vivo* Raman spectroscopy

Living *Pocillopora damicornis* and *Acropora yongei* corals, and a benthic foraminifer (*Amphisorus* sp.) were collected from Rottnest Island in Western Australia (32.02°S, 115.52°E; see Ross et al. (2015) for a detailed map of the study area). Two different *A. yongei* colonies were used (hereafter referred to as *A. yongei* 1 and 2). Additionally, living coralline algae (*Hydrolithon reinboldii*) were collected from Tallon Island in the Kimberley region of Western Australia (16.41°S, 123.12°E; see Cornwall et al. (2018) for collection details). All specimens were maintained in plastic or glass aquaria at the Waterman's Bay marine research facility of the University of Western Australia. Branch tips (1-2 cm) of the two coral species were broken from each colony, whereas the entire living foraminifer was used for *in vivo* analyses. The *Hydrolithon reinboldii* specimens produced offspring that recruited onto the sides of plastic aquaria, and a piece of an aquarium containing a living recruit was removed for subsequent analysis.

2.1.2 Specimens for high-resolution *ex vivo* Raman spectroscopy mapping

A living colony of *Stylophora pistillata* was collected at 2 m depth from Ningaloo Reef near Coral Bay, Western Australia, the tissue removed with a water jet, and the skeleton dried in an oven at 50 °C for 24 hours. A branch tip was broken from the skeleton and a petrographic thin section was prepared.

A deep-sea cup coral, *Desmophyllum dianthus*, was collected from a depth of 675 m within the Antarctic Intermediate Waters of the Perth Canyon offshore Western Australia, during the oceanographic cruise FK20150301 (31.55°S, 115.05°E; see Trotter et al., 2018). The coral was soaked in purified (Milli-Q) water for several hours to remove organic tissue, and the skeleton was then dried overnight in an oven at 40 °C. A septum and the adjacent wall was removed using a dental drill and diamond disk, set in epoxy resin, polished to expose the calcification centers, and sonicated in Milli-Q water and then AR grade methanol.

The coralline alga *Sporolithon durum* was collected from Bremer Bay (34.4°S, 119.4°E; see Ross et al. (2018) for a description of the collection site).

A juvenile planktonic foraminifer, *Orbulina universa*, was collected off the coast of New South Wales, Australia and cultured in the laboratory at Australian National University during 2007 following the protocol described in Hori et al. (2018). The specimen formed a spherical chamber in the aquarium and underwent gametogenesis eight days later. The shell of the *O. universa* specimen was cleaned in deionized water and embedded in resin for Raman spectroscopy. The distribution of Mg in this shell was previously mapped using NanoSIMs (Spero et al., 2015).

Finally, we used a sagittal otolith from a coral reef fish (*Pseudochromis fuscus*) caught on Ningaloo Reef. Annual bands in the otolith were used in a previous study to identify specimen age (Thillainath et al., 2016). The sample was previously cut and ground with a flat surface glued to a glass slide. We conducted our Raman measurements through the glass slide to image the flat face cut through the center of the otolith.

142 **2.2 *in vivo* Raman spectroscopy**

143 Raman spectroscopy measurements were made *in vivo* on coral (*P. damicornis* and *A.*
144 *yongei*), a coralline alga (*H. reinboldii*), and a benthic foraminifer (*Amphisorus* sp.). Each
145 specimen was placed in seawater (sourced from Waterman's Bay, Western Australia), either
146 in a petri dish (foraminifer), or in a cup with a water-circulating pump that was turned off
147 several minutes prior to Raman measurements. Generally, Raman spectra were collected in
148 the dark, although measurements in the light are also possible (see Supporting Material
149 Figure S1). Measurements were made with a WITec Alpha300 RA+ confocal Raman
150 microscope system with a 785 nm laser source, a 20X submersible objective with 0.5
151 aperture, a CCD detector maintained at -60 °C, and either a 600 or 1200 mm^{-1} grating.
152 Different gratings were used to test if the method was generalizable because some
153 applications may require the broader spectral coverage of a 600 mm^{-1} grating (*e.g.* to identify
154 "lattice-mode" peaks; Dandeu et al., 2006), despite its lower spectral resolution (discussed
155 below). Repeated analyses of a silicon chip were conducted for wavenumber calibration, and
156 reported wavenumbers have been calibrated to the primary silicon peak at 520.7 cm^{-1}.

157 Living specimens were placed in seawater and examined under the microscope. The
158 objective was lowered into and then raised out of the seawater several times to remove air
159 bubbles on the lens before final submersion into the seawater. Initially, the focal plane was
160 set near the outer tissue layer of each specimen under bright-field illumination. Next, the
161 laser was turned on and Raman spectra were recorded every 3 to 5 seconds while
162 incrementally moving the focus downwards into the tissue and towards the skeletons (Fig.
163 1a-c). The intensity of the ν_1 peak, which represents the symmetric stretching of C-O bonds
164 in all $CaCO_3$ minerals, was used to identify the location of the skeleton surface. We assumed
165 that the spectrum with maximum intensity of the ν_1 peak corresponded to where the confocal
166 plane was most closely aligned with the top of the skeleton (Fig. 1d-e). For corals, we used

the peak width (full width at half maximum intensity, or FWHM; see Fig. 1) of the ν_1 peak to determine Ω_{Ar} of the calcifying fluid from which the skeleton recently formed, based on the previously described calibration between FWHM and Ω_{Ar} of abiogenic aragonites (DeCarlo et al., 2017). This calibration is based on the finding that aragonite precipitating from higher supersaturation is more disordered (higher FWHM) due to either incorporation of impurities or lattice defects that occur under rapid crystallization. For the calcitic foraminifer and coralline alga, we used the ν_1 peak wavenumber to estimate the skeleton %Mg (Borromeo et al., 2017; Perrin et al., 2016). Additionally, we calculated the residual FWHM between measured FWHM and that calculated based on a calibration between FWHM and %Mg (Perrin et al., 2016).

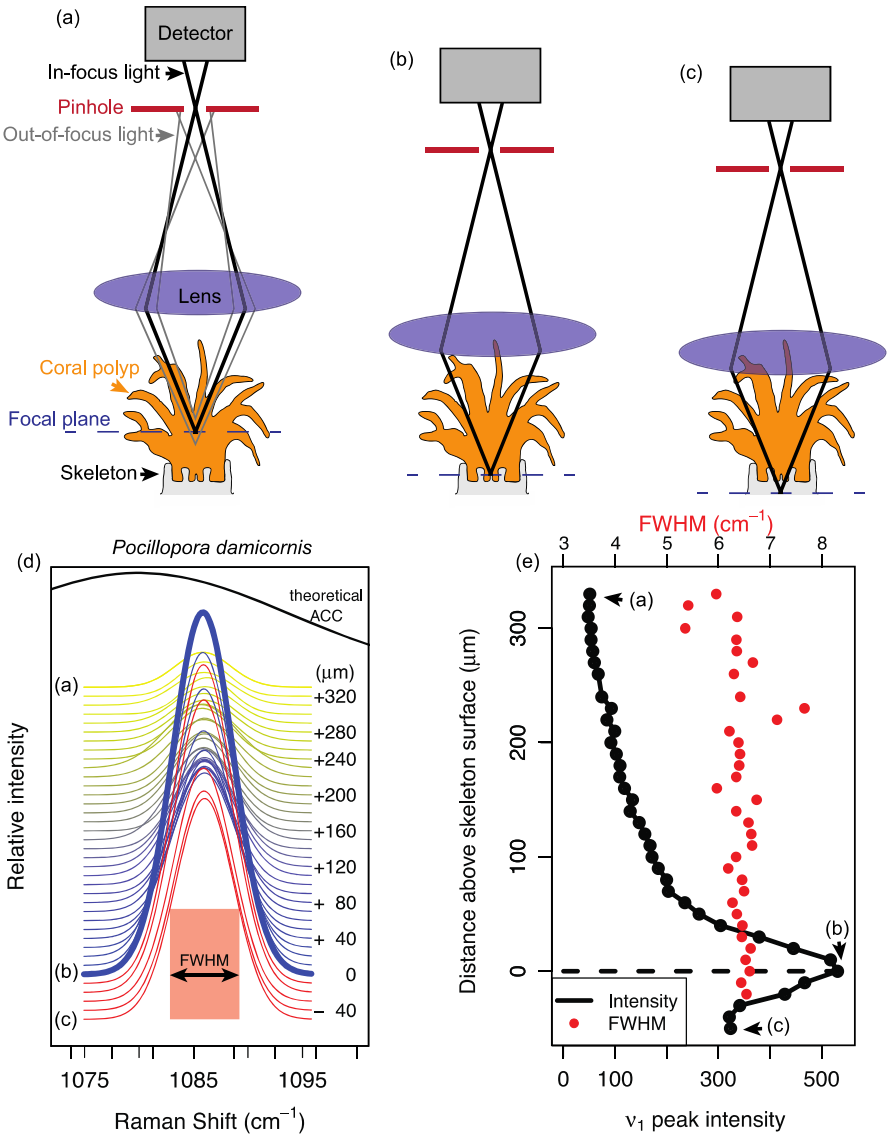

Figure 1. Schematic illustrating *in vivo* Raman profiling of living corals. (a) Initially, the Raman system is focused near the outer tissue layer. A pinhole (red) in the confocal Raman microscope blocks out-of-focus light (gray lines), allowing only in-focus light (black lines) from a narrow focal plane (blue dashed line) to reach the detector. As the microscope objective is lowered, the focal plane reaches the skeleton (b) and then the focal plane extends slightly beneath the skeletal surface (c). (d) Raman ν_1 peaks collected as the microscope focus moved from the outer tissue to the skeleton (yellow to blue), and out of focus beneath the skeletal surface (red). The thick blue line corresponds to the spectrum with the greatest ν_1 peak height. The letters to the left of the peaks correspond to schematic panels (a-c) above,

and the numbers to the right of the peaks indicate the distance of the focal plane above the skeleton surface. The black curve shows the expected appearance of an amorphous calcium carbonate (ACC) peak based on Wang et al. (2012). (e) Intensity of the ν_1 peak (black) and its Full Width at Half Maximum (FWHM; red) for the spectra shown in (d). The detection of the ν_1 peak and its FWHM through the coral polyp arises from weak signals of scattered and/or out-of-focus light, not from aragonite crystals within the tissue.

2.3 Evaluation of potential effects of seawater on carbonate ν_1 FWHM

We tested whether immersing coral skeletons in seawater influenced the Raman ν_1 peak. Specifically, we tested whether ν_1 FWHM of a single sample was different when measured in air or seawater. We placed a *Porites* sp. coral skeleton in an empty cup and collected 10 Raman spectra with the 1200 mm^{-1} grating and the submersible objective. Next, we filled the cup with seawater without moving the skeleton or adjusting the microscope focus, and collected an additional 10 spectra.

2.4 High-resolution *ex vivo* Raman spectroscopy mapping

Samples for high-resolution *ex vivo* mapping were analyzed with the same Raman system, except using a non-submersible 20X objective with a 0.5 numerical aperture. All measurements were made with a 1200 mm^{-1} grating. Spatial resolution ranged from 0.25 to 15 μm, and integration times from 0.3 to 2.5 s, depending on the sample (Supporting Material Table S1). As with the *in vivo* measurements, we used ν_1 FWHM as a proxy for Ω_{Ar} in corals, and for calcitic samples we calculated the %Mg (from ν_1 wavenumber), ν_1 FWHM, and ν_1 residual FWHM (after accounting for Mg).

2.5 NanoSIMS

We used nanoscale secondary ion mass spectrometry (NanoSIMS) to map the distribution of Mg/Ca in the *S. pistillata* coral and *O. universa* foraminifer. These were the

two specimens mapped with Raman at sufficiently small scales to compare directly with NanoSIMS. The NanoSIMS maps serve to confirm the presence of micro-banding features in these samples, and especially to validate the interpretation of Mg/Ca in the foraminifer. Details of the NanoSIMS measurements can be found in the Supporting Material.

3. Results

3.1 Effects of seawater on carbonate ν_1 FWHM

The carbonate ν_1 FWHM of the *Porites* sp. skeleton measured in air was 3.214 ± 0.003 (1 σ) cm^{-1}, which translates to Ω_{Ar} of 7.2 ± 0.1 (DeCarlo et al., 2017). In comparison, ν_1 FWHM of the same *Porites* sp. skeleton measured in seawater was 3.24 ± 0.01 cm^{-1}, or a Ω_{Ar} of 7.6 ± 0.2. A two-sample t-test showed that the difference in FWHM was significant ($p < 0.05$), although the difference in derived Ω_{Ar} was relatively small (0.4 Ω_{Ar} units). The greater FWHM from the measurements conducted in seawater is potentially due to a slight increase in instrument noise due to the scattered light passing through the seawater medium, as instrument noise is known to increase FWHM (DeCarlo et al., 2017; Nasdala et al., 2001). It is also possible that the seawater may have refracted the light to a different point on the skeleton surface, even though the sample itself was not moved. Thus, while there is potential for slight artificial increases in FWHM when conducting Raman spectroscopy measurements in seawater, the effect is relatively small and would be negligible for comparison of samples measured underwater.

3.2 *in vivo* Raman spectroscopy of marine calcifying organisms

Raman spectroscopy profiles conducted from the outer tissue layer downwards produced distinct maxima of ν_1 peak intensity within hundreds of microns (Fig. 1e and Fig. 2a-d). Analyses of the *P. damicornis* and the first *A. yongei* ("*A. yongei* 1") coral specimens were conducted with a 600 mm^{-1} grating, which is less effective for quantifying Ω_{Ar} due to

238 the lower spectral resolution but captures a larger range of Raman shifts. Nevertheless, the ν_1
239 FWHM of the spectra focused on the skeletal surfaces were 6.6 and 6.7 cm^{-1}, respectively,
240 which is consistent with $\Omega_{Ar} < 20$ (DeCarlo et al., 2017). The second *A. yongei* ("*A. yongei*
241 2") specimen was analyzed with a 1200 mm^{-1} grating, and its ν_1 FWHM was 3.40 cm^{-1},
242 equivalent to Ω_{Ar} of 10 (DeCarlo et al., 2017). This is generally similar to that measured on
243 *Acropora* skeletal samples (Comeau et al., 2018; DeCarlo et al., 2017, 2018), albeit on the
244 lower end of the previously reported range. For the coralline alga *H. reinboldii*, the ν_1
245 wavenumber was 1088.63 cm^{-1}, which corresponds to a Mg content of 10.8% (Perrin et al.,
246 2016). The measured ν_1 FWHM was 9.5 cm^{-1}, compared to an expected FWHM of 8.2 cm^{-1}
247 based on the Mg content (Perrin et al., 2016), leaving a "residual FWHM" of 1.3 cm^{-1}.
248 Consistent with this result, three previous studies of coralline algae skeletons calculated
249 residual FWHM in the same way and reported values ranging from approximately 0.3 to 1.6
250 cm^{-1} (Comeau et al., 2018; Cornwall et al., 2018; McCoy & Kamenos, 2018). The
251 *Amphisorus* sp. foraminifer had a ν_1 wavenumber of 1089.15 cm^{-1} (13.3% Mg), a measured
252 FWHM of 8.83 cm^{-1}, and a residual FWHM of -0.17 cm^{-1}.
253 Inspection of the ν_1 and ν_4 peaks following previous studies (Dandeu et al., 2006;
254 DeCarlo et al., 2015; Perrin et al., 2016; Wehrmeister et al., 2009) clearly revealed that all the
255 corals are solely aragonitic, and both the coralline alga and the foraminifer are solely calcitic,
256 with no other mineral phases detected in any of the profiles (Fig. 2e-l). The ν_4 peak of
257 aragonite is a doublet centered at approximately 705 cm^{-1} (Dandeu et al., 2006), although the
258 two peaks were distinguishable only with the 1200 mm^{-1} grating (Fig. 2f) but not the 600
259 mm^{-1} grating (Fig. 2e). Regardless of the spectral resolution (600 mm^{-1} versus 1200 mm^{-1}
260 gratings), the wavenumbers of the ν_1 and ν_4 peaks of all spectra in the coral profiles (Fig.
261 2e,f,i,j) were consistent with aragonite. While the spectra from the coral profiles showed
262 some increase in intensity between 720 cm^{-1} and 750 cm^{-1}, the region where peaks for other

carbonate minerals may be expected, there were no distinct peaks observed. Furthermore, there were no signs of any other ν_1 peaks besides aragonite, suggesting that the slightly increased intensity between 720 cm^{-1} and 750 cm^{-1} is only an increase in the background, potentially due to fluorescence. The ν_1 and ν_4 peaks of the foraminifer and coralline alga profiles were clearly consistent with the sole presence of high-Mg calcite. The profiles of all the organisms also showed no evidence of ACC. The absence of ACC is most clearly revealed in that the ν_1 FWHM are all less than 11 cm^{-1} (Fig. 2a-d), which is unambiguously distinct from the FWHM of > 20 cm^{-1} for ACC (Wang et al., 2012) (see also Fig. 1d).

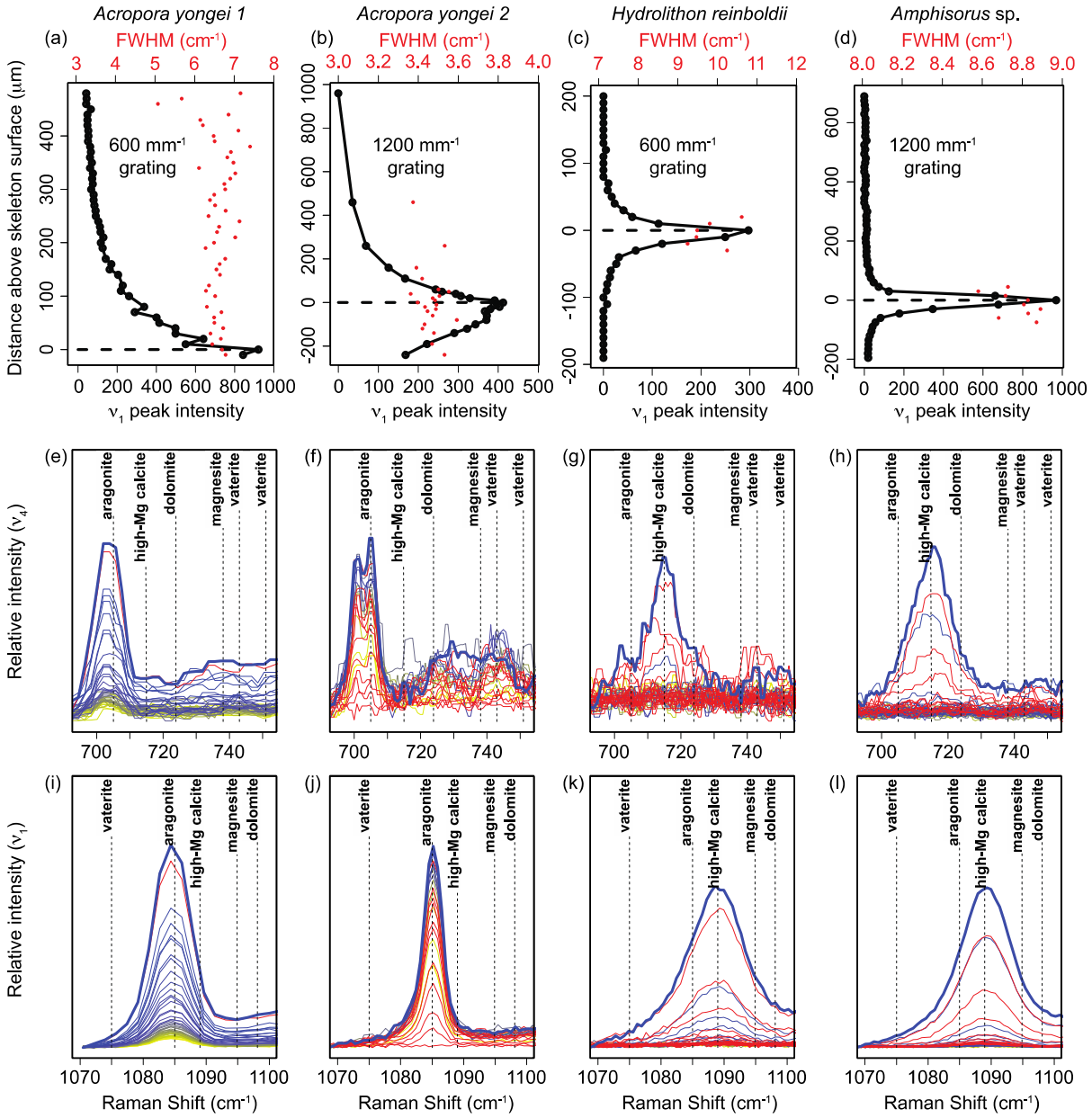

Figure 2. Application of *in vivo* Raman profiling to coral (*A. yongei*; a,b,e,f,i,j), a coralline alga (*H. reinboldii*; c,g,k), and a foraminifer (*Amphisorus* sp.; d,h,l). (a-d) Profiles of ν_1 peak intensity (black) and FWHM (red) (see Fig. 1 schematic for additional details). The ν_1 (e-h) and ν_4 (i-l) peaks clearly reveal the two corals are aragonitic and both the coralline alga and forminifer are calcitic. Colors in (e-l) follow the same scheme as in Fig. 1d, with yellow to blue colors showing the transition from focus on the outer tissue to the skeleton, and red indicating out-of-focus below the skeletal surface. Peak positions for calcite (assuming 10%

Mg), magnesite, and dolomite are based on Perrin et al. (2016) and the peaks for vaterite are based on Wehrmeister et al. (2009) and Melancon et al. (2008).

3.3 High-resolution *ex vivo* Raman mapping of marine calcifying organisms

Raman *ex vivo* mapping of corals, a fish otolith, a foraminifer, and a coralline alga revealed 10-100 μm banding patterns in each organism (Fig. 3). For corals, micro-banding patterns are reflected in the calcifying fluid Ω_{Ar} (derived from ν_1 FWHM). The ~10-20 μm wide oscillations of Ω_{Ar} in the *S. pistillata* specimen (Fig. 3b) may reflect daily bands. Additionally, we observed elevated Ω_{Ar} at the centers of calcification (COCs; the yellow band indicating high Ω_{Ar} in the center of the skeletal spine in Fig. 3d), consistent with previous Raman analyses of *P. damicornis* (DeCarlo, Ren, & Farfan, 2018) and *Porites lutea* (Wall & Nehrke, 2012). The deep-sea cup coral, *D. dianthus*, showed complex patterns of Ω_{Ar}, with a central axis of centers of calcification in addition to fine-scale Ω_{Ar} banding throughout the skeleton (Fig. 3e). While these banding patterns are of unknown temporal frequency, we note that deep-sea corals grow their skeletons relatively slowly, with *Desmophyllum* annual extension rates ranging from 0.1 to 3 mm yr^{-1} (Adkins et al., 2004; Cheng et al., 2000; Risk et al., 2002).

The fish otolith contained distinct banding patterns in ν_1 peak intensity (Fig. 3f). These bands may reflect both daily (near the nucleus) and annual (broader bands near the outer edge) growth accretions. Since the otolith is aragonite, ν_1 FWHM could potentially be used to quantify Ω_{Ar}, however the published FWHM-Ω_{Ar} calibration was based on aragonite precipitating from seawater (DeCarlo et al., 2017). Corals likely precipitate aragonite from a seawater-sourced solution (DeCarlo et al., 2017; Gagnon, Adkins, & Erez, 2012) with the elemental composition of their skeletons being similar to aragonite precipitated from

seawater (DeCarlo et al., 2015; Gonneea et al., 2017; Holcomb et al., 2009). Conversely, otoliths mineralize from fluids tightly regulated by the fish, and their elemental composition is distinct from corals (Campana, 1999; Hathorne et al., 2013; Sturgeon et al., 2005; Yoshinaga et al., 2000). Therefore, we present the otolith ν_1 FWHM in its measured units rather than deriving Ω_{Ar} (Fig. 3g). The variability of FWHM is dominated by a pattern of high FWHM in the nucleus and decreasing toward the outer edges, with some subtle banding superimposed onto this trend.

Raman analyses of calcitic specimens can also be used to estimate the molar %Mg by quantifying the wavenumber (*i.e.* position) of the ν_1 peak (Perrin et al., 2016). In fact, the Mg content must be quantified before interpreting FWHM of calcite because the incorporation of varying amounts of Mg can impose changes in FWHM independent of other factors (Perrin et al., 2016). Our calcitic foraminifer (*O. universa*) and coralline alga (*S. durum*) exhibited clear banding patterns in ν_1 wavenumber on spatial scales of order 10 μm (Fig. 3 h,k). Using an abiogenic calibration of ν_1 wavenumber to %Mg (Perrin et al., 2016), these bands corresponded to Mg contents of approximately 0.5-3% in the foraminifer and 15-20% in the coralline alga. These estimates are generally consistent with previous measurements of Mg content in these species (A. M. Smith et al., 2012; Spero et al., 2015). Measured ν_1 FWHM showed a nearly identical pattern to %Mg (Fig. 3i,l), consistent with the notion that calcite ν_1 FWHM variability can be dominated by the influence of Mg (see also Supporting Material Figure S2). Indeed, most of the ν_1 FWHM banding disappeared when we calculated the residual FWHM (after removing the effect of Mg) (Fig. 3m), yet some variations remain, such as a general decrease in residual FWHM from the bottom to the top of the map of the coralline alga. NanoSIMS Mg/Ca showed similar banding patterns as FWHM in the *S. pistallata* coral and in the *O. universa* foraminifer (Fig. 3).

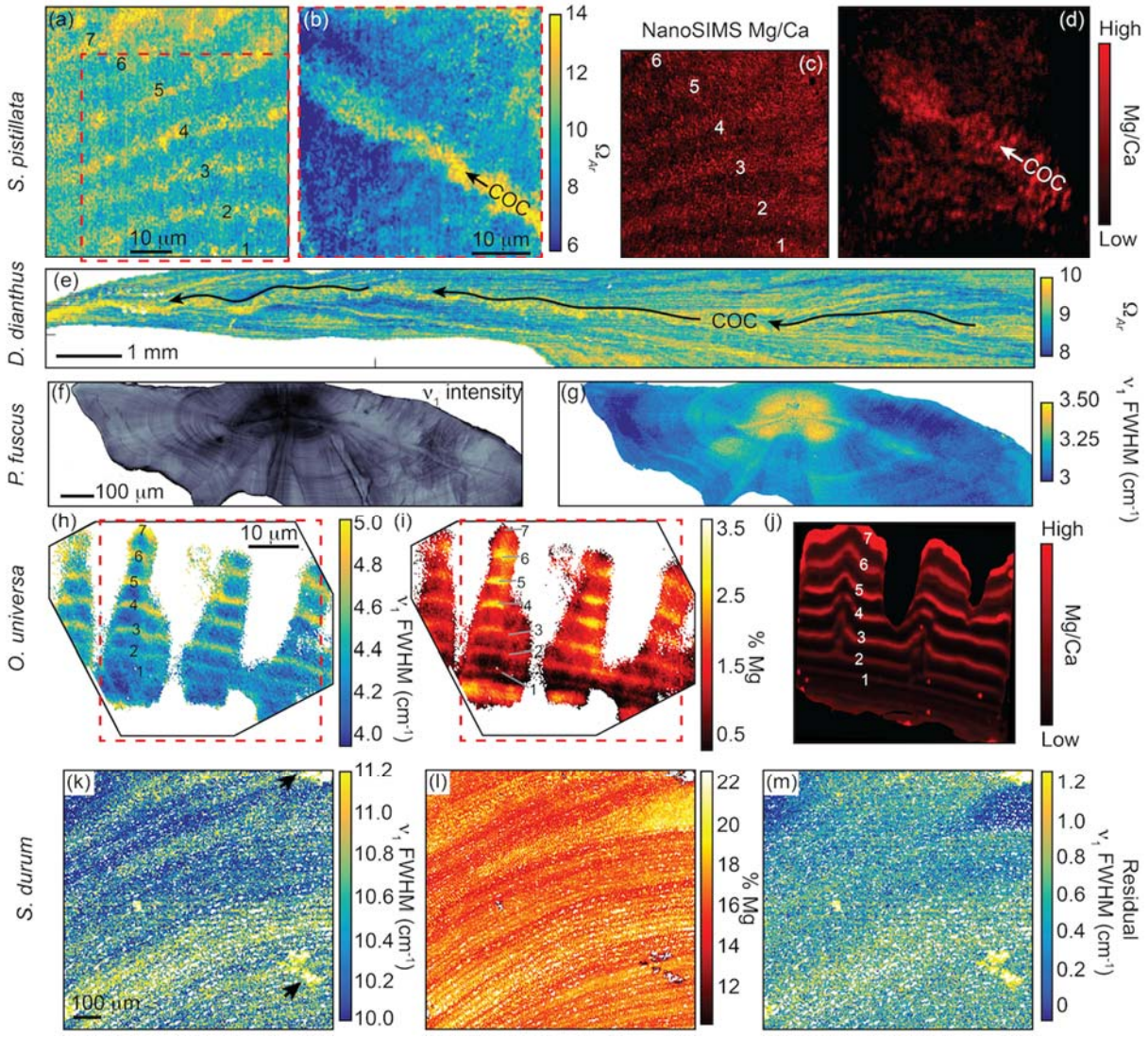

Figure 3. High-resolution *ex vivo* Raman mapping of various marine calcifying organisms. (a-d) Shallow water coral (*S. pistillata*) with Ω_{Ar} mapped from ν_1 FWHM (a,b), and Mg/Ca mapped with NanoSIMS (c,d; corresponding to a,b, respectively). (e) Deep-sea coral (*D. dianthus*) Ω_{Ar}. (f,g) Fish otolith (*P. fuscus*) maps of ν_1 intensity (f) and ν_1 FWHM (g). (h-j) Foraminifer (*O. universa*) ν_1 FWHM (h), %Mg (i, from ν_1 wavenumber), and relative Mg/Ca (j, from NanoSIMS). (k-m) Coralline alga *S. durum* ν_1 FWHM (k), %Mg (l, from ν_1 wavenumber), and ν_1 residual FWHM (m, after accounting for the effect of Mg). Arrows in (k) indicate locations of minor aragonite presence. Red dashed boxes in a,b,h,i indicate the locations of NanoSIMS mapping. Numbers in the *S. pistillata* and *O. universa* maps aid in

matching bands between images. “COC” indicates centers of calcification in the coral maps. Apparent differences in the shape of the foraminifer shell between Raman and NanoSIMS images are due to slight variations in the surface exposed to each measurement.

---

4. Discussion

We present Raman spectroscopy techniques for investigating marine bio-calcification mechanisms. With both *in vivo* and high-resolution *ex vivo* mapping procedures, we show that Raman spectroscopy is a powerful tool for characterizing the mineralogy of a variety of marine calcifying organisms. Our initial applications demonstrate that Raman spectroscopy is suitable to address a range of questions at the forefront of current knowledge of marine bio-calcification.

Raman spectroscopy has recently been applied to quantify the response of corals, coralline algae, and fish otoliths to simulated ocean acidification (Coll-Lladó et al., 2018; Comeau et al., 2018; Cornwall et al., 2018; DeCarlo et al., 2017, 2018; Foster & Clode, 2016; Kamenos et al., 2013, 2016). While these studies have revealed changes in both the mineralogy and disorder of calcified structures under ocean acidification, they have so far conducted Raman spectroscopy analyses of powders or made spot measurements on intact samples. Here, we extend the application of Raman spectroscopy for investigating marine bio-calcification responses to environmental change with both *in vivo* and high-resolution mapping.

Previous Raman studies utilizing spot measurements can resolve mineralogical changes in calcified structures on spatial scales of at least tens to hundreds of μm and on temporal scales of seasons or longer (*e.g.* Ross et al., 2018). Our *in vivo* approach enables quantification of mineralogies as well as calcifying fluid Ω_{Ar} of corals, on a timescale of

seconds. This advance can help to resolve the problem of differing temporal and spatial scales among techniques used in coral calcification studies (Holcomb et al., 2014). Although geochemical (*i.e.* isotopic and elemental) analyses of coral skeletons are effective at deriving the carbonate system of the calcifying fluid (DeCarlo, Holcomb, & McCulloch, 2018; McCulloch et al., 2017), such studies have been difficult to reconcile with alternative approaches based on inserting micro-sensors into the coral calcifying fluid (Al-Horani, Al-Moghrabi, & De Beer, 2003; Cai et al., 2016; Ries, 2011), or imaging the calcifying fluid of corals exposed to pH-sensitive dyes (Comeau et al., 2017; Holcomb et al., 2014; Venn et al., 2011). Conversely, Raman spectroscopy can now be applied *in vivo* at temporal and spatial scales comparable to the micro-sensor studies (Fig. 1), as well as to bulk powders for comparison to isotopic measurements (*e.g.* DeCarlo et al., 2017, 2018). Recent development of microfluidic chambers for live-imaging of coral polyps–"coral-on-a-chip"–(Shapiro et al., 2016), could also be readily utilized with *in vivo* Raman spectroscopy to test acute responses of coral calcifying fluid Ω_{Ar} and mineralogy to manipulations of seawater chemistry and temperature.

In vivo Raman spectroscopy is especially well-suited to address the recent debate regarding whether corals precipitate their aragonite skeletons directly from seawater or via transformation of ACC particles (DeCarlo, 2018; DeCarlo, Ren, & Farfan, 2018; Mass et al., 2017; Von Euw et al., 2017). Mass et al. (2017) reported ACC in *S. pistillata* based on photoemission electron microscopy (PEEM), although the ACC was only observed in trace amounts on some outer edges of the skeleton, thus leaving open the possibility that it was an artefact of preparation techniques (including dehydrating the coral, and cutting, grinding, polishing, and embedding the skeleton). Conversely, *in vivo* Raman spectroscopy does not sacrifice the coral and does not require any preparation of the skeleton, and ACC is easily distinguishable in Raman spectra (Fig. 1d). This makes *in vivo* Raman the ideal technique for

390 determining whether ACC is present in corals. Thus, our finding that ACC was clearly absent
391 from all our *in vivo* profiles (Fig. 2) is key evidence supporting the notion that corals directly
392 precipitate aragonite. While it is important to emphasize that this lack of evidence is not
393 necessarily proof for the complete absence of transient ACC in coral calcification, it indicates
394 that if present, ACC is below the detection limits of our current approach. Importantly, our
395 initial results demonstrate the benefits and ability of Raman spectroscopy to address this
396 question.

397 High-resolution *ex vivo* Raman mapping provides a complementary approach to *in vivo*
398 profiling. While our *in vivo* technique provides a snapshot of mineralogy at a single point in
399 time and space, *ex vivo* mapping reveals the spatial variability of mineralogy and disorder
400 within shells and skeletons (Nehrke, Nouet, & Treude, 2011; Roger et al., 2017; Wall &
401 Nehrke, 2012; Wall et al., 2015), including banding patterns representing a range of
402 timescales from days to years (Fig. 3). Like our *in vivo* profiling results, high-resolution *ex*
403 *vivo* mapping showed that the corals and fish otolith are composed entirely of aragonite,
404 whereas the foraminifer and coralline alga are entirely calcitic, except for minor aragonite
405 contamination or infilling in the coralline alga. The banding of ν_1 peak intensity in the fish
406 otolith may be due to differing proportions of organics and aragonite crystals (Jolivet et al.,
407 2008, 2013). Conversely, micro-banding patterns in the aragonitic corals are likely caused by
408 variations in calcifying fluid Ω_{Ar}, which could also explain the Mg/Ca banding observed here
409 (Fig. 3c,d) and described previously (Meibom et al., 2004) because aragonite Mg/Ca
410 increases with Ω_{Ar} or crystal growth rate (AlKhatib & Eisenhauer, 2017; DeCarlo et al.,
411 2017). Raman bands in the calcitic foraminifer and coralline alga are dominated by the
412 effects of Mg (Fig. 3), but it is not yet clear if the Mg banding arises from temporal changes
413 in carbonate chemistry or intrinsic biological rhythms (Fehrenbacher et al., 2017; Spero et al.,
414 2015). Nevertheless, that our Raman-based visualization of Mg banding in the foraminifer is

similar to that from NanoSIMS suggests that Raman spectroscopy can be used as a rapid and cost-effective technique to map the distribution of Mg in calcitic shells and skeletons.

In summary, Raman spectroscopy adds substantially to the toolbox of techniques available for studying marine bio-calcification (see Box 1). Among the greatest advantages of Raman spectroscopy is its applicability on small spatial and temporal scales, enabling characterization of near-instantaneous skeletal growth and micro-banding patterns produced on various timescales. Although our initial applications provided no evidence for a role of ACC particles in calcification by a range of taxa, Raman spectroscopy can now be readily applied to search for ACC in various developmental stages and under different environmental conditions (Akiva et al., 2018; Foster & Clode, 2016). Organic matrices may also play an important role in calcification for some taxa, and Raman spectroscopy has been used to characterize their distribution in shells and skeletons (DeCarlo, Ren, & Farfan, 2018; Jolivet et al., 2013; Nehrke, Nouet, & Treude, 2011; Von Euw et al., 2017). Furthermore, studies of simulated ocean acidification and warming can quantify changes in calcifying fluid Ω_{Ar} of corals, and mineralogy of coralline algae and foraminifera, without sacrificing experimental replicates (Box 1). For example, *in vivo* Raman profiling could be conducted repeatedly (*e.g.* daily) on the same individuals in treatment conditions for weeks to months to assess acclimatization, or on parents and offspring to assess adaptive responses. Since acclimatization and adaptation likely represent critical components of biological responses to global climate change (*e.g.* Schoepf et al., 2017), studying them with Raman spectroscopy will be a valuable research direction.

Acknowledgements

The authors acknowledge the facilities, and the scientific and technical assistance of the Australian Microscopy & Microanalysis Research Facility at the Centre for Microscopy,

Characterisation & Analysis, The University of Western Australia, a facility funded by the University, State and Commonwealth Governments. The authors also acknowledge Microscopy Australia, AuScope, the Science and Industry Endowment Fund, and the State Government of Western Australian for contributing to the Ion Probe Facility at the University of Western Australia. The Australian Research Council is acknowledged for fellowship funding to J.A.T (FT160100259) and M.T.M (FL120100049). S.C. was supported by an ARC DECRA (DE160100668). A.S. is thankful for support from Prof. Stephen Eggins and Dr. Katsunori Kimoto while undertaking foraminifera culturing experiments. The authors declare no conflicts of interest.

References

Adkins, J. F., Henderson, G. M., Wang, S.-L., O'Shea, S., & Mokadem, F. (2004). Growth rates of the deep-sea scleractinia Desmophyllum cristagalli and Enallopsammia rostrata. *Earth and Planetary Science Letters*, *227*(3–4), 481–490. https://doi.org/10.1016/J.EPSL.2004.08.022

Akiva, A., Neder, M., Kahil, K., Gavriel, R., Pinkas, I., Goobes, G., & Mass, T. (2018). Minerals in the pre-settled coral Stylophora pistillata crystallize via protein and ion changes. *Nature Communications*, *9*(1), 1880. https://doi.org/10.1038/s41467-018-04285-7

Al-Horani, F. A., Al-Moghrabi, S. M., & De Beer, D. (2003). The mechanism of calcification and its relation to photosynthesis and respiration in the scleractinian coral Galaxea fascicularis. *Marine Biology*, *142*(3), 419–426. https://doi.org/10.1007/s00227-002-0981-8

AlKhatib, M., & Eisenhauer, A. (2017). Calcium and Strontium Isotope Fractionation during Precipitation from Aqueous Solutions as a Function of Temperature and Reaction Rate;

II. Aragonite. *Geochimica et Cosmochimica Acta*, *209*, 320–342. https://doi.org/10.1016/j.gca.2017.04.012

Berelson, W. M., Balch, W. M., Najjar, R., Feely, R. A., Sabine, C., & Lee, K. (2007). Relating estimates of CaCO 3 production, export, and dissolution in the water column to measurements of CaCO 3 rain into sediment traps and dissolution on the sea floor: A revised global carbonate budget. *Global Biogeochemical Cycles*, *21*(1). https://doi.org/10.1029/2006GB002803

Borromeo, L., Zimmermann, U., Andò, S., Coletti, G., Bersani, D., Basso, D., … Garzanti, E. (2017). Raman spectroscopy as a tool for magnesium estimation in Mg-calcite. *Journal of Raman Spectroscopy*, *48*(7), 983–992. https://doi.org/10.1002/jrs.5156

Cai, W.-J., Ma, Y., Hopkinson, B. M., Grottoli, A. G., Warner, M. E., Ding, Q., … Wang, Y. (2016). Microelectrode characterization of coral daytime interior pH and carbonate chemistry. *Nature Communications*, *7*, 11144. https://doi.org/10.1038/ncomms11144

Campana, S. E. (1999). Chemistry and composition of fish otoliths: pathways, mechanisms and applications. *Marine Ecology Progress Series*. Inter-Research Science Center. https://doi.org/10.2307/24853344

Cheng, H., Adkins, J., Edwards, R. L., & Boyle, E. A. (2000). U-Th dating of deep-sea corals. *Geochimica et Cosmochimica Acta*, *64*(14), 2401–2416. https://doi.org/10.1016/S0016-7037(99)00422-6

Coll-Lladó, C., Giebichenstein, J., Webb, P. B., Bridges, C. R., & de la serrana, D. G. (2018). Ocean acidification promotes otolith growth and calcite deposition in gilthead sea bream (Sparus aurata) larvae. *Scientific Reports*, *8*(1), 8384. https://doi.org/10.1038/s41598-018-26026-y

Comeau, S., Cornwall, C. E., DeCarlo, T. M., Krieger, E., & McCulloch, M. T. (2018). Similar controls on calcification under ocean acidification across unrelated coral reef

taxa. *Global Change Biology*, *24*(10), 4857–4868. https://doi.org/10.1111/gcb.14379

Comeau, S., Tambutté, E., Carpenter, R. C., Edmunds, P. J., Evensen, N. R., Allemand, D., … Venn, A. A. (2017). Coral calcifying fluid pH is modulated by seawater carbonate chemistry not solely seawater pH. *Proceedings of the Royal Society of London B: Biological Sciences*, *284*(1847).

Cornwall, C. E., Comeau, S., DeCarlo, T. M., Moore, B., D'Alexis, Q., & McCulloch, M. T. (2018). Resistance of corals and coralline algae to ocean acidification: physiological control of calcification under natural pH variability. *Proceedings of the Royal Society B: Biological Sciences*, *285*(1884), 20181168. https://doi.org/10.1098/rspb.2018.1168

Dandeu, A., Humbert, B., Carteret, C., Muhr, H., Plasari, E., & Bossoutrot, J. M. (2006). Raman Spectroscopy – A Powerful Tool for the Quantitative Determination of the Composition of Polymorph Mixtures: Application to CaCO3 Polymorph Mixtures. *Chemical Engineering & Technology*, *29*(2), 221–225. https://doi.org/10.1002/ceat.200500354

DeCarlo, T. M. (2018). Characterizing coral skeleton mineralogy with Raman spectroscopy. *Nature Communications*, *9*(1), 5325. https://doi.org/10.1038/s41467-018-07601-3

DeCarlo, T. M., Comeau, S., Cornwall, C. E., & McCulloch, M. T. (2018). Coral resistance to ocean acidification linked to increased calcium at the site of calcification. *Proceedings of the Royal Society B: Biological Sciences*, *285*(1878), 20180564. https://doi.org/10.1098/rspb.2018.0564

DeCarlo, T. M., D'Olivo, J. P., Foster, T., Holcomb, M., Becker, T., & McCulloch, M. T. (2017). Coral calcifying fluid aragonite saturation states derived from Raman spectroscopy. *Biogeosciences*, *14*(22), 5253–5269. https://doi.org/10.5194/bg-14-5253-2017

DeCarlo, T. M., Gaetani, G. A., Holcomb, M., & Cohen, A. L. (2015). Experimental

515 determination of factors controlling U/Ca of aragonite precipitated from seawater:
516 implications for interpreting coral skeleton. *Geochimica et Cosmochimica Acta*, *162*,
517 151–165. https://doi.org/doi:10.1016/j.gca.2015.04.016
518 DeCarlo, T. M., Holcomb, M., & McCulloch, M. T. (2018). Reviews and syntheses:
519 Revisiting the boron systematics of aragonite and their application to coral calcification.
520 *Biogeosciences Discussions*, 1–20. https://doi.org/10.5194/bg-2018-77
521 DeCarlo, T. M., Ren, H., & Farfan, G. (2018). The origin and role of organic matrix in coral
522 calcification: insights from comparing coral skeleton and abiogenic aragonite. *Frontiers*
523 *in Marine Science*, *5*, 170. https://doi.org/10.3389/FMARS.2018.00170
524 Fehrenbacher, J. S., Russell, A. D., Davis, C. V., Gagnon, A. C., Spero, H. J., Cliff, J. B., …
525 Martin, P. (2017). Link between light-triggered Mg-banding and chamber formation in
526 the planktic foraminifera Neogloboquadrina dutertrei. *Nature Communications*, *8*,
527 15441. https://doi.org/10.1038/ncomms15441
528 Foster, T., & Clode, P. L. (2016). Skeletal mineralogy of coral recruits under high
529 temperature and pCO2. *Biogeosciences*, *13*, 1717–1722. https://doi.org/10.5194/bg-13-
530 1717-2016
531 Gagnon, A. C., Adkins, J. F., & Erez, J. (2012). Seawater transport during coral
532 biomineralization. *Earth and Planetary Science Letters*, *329*, 150–161.
533 Gonneea, M. E., Cohen, A. L., DeCarlo, T. M., & Charette, M. A. (2017). Relationship
534 between water and aragonite barium concentrations in aquaria reared juvenile corals.
535 *Geochimica et Cosmochimica Acta*, *209*, 123–134.
536 https://doi.org/10.1016/j.gca.2017.04.006
537 Hathorne, E. C., Gagnon, A., Felis, T., Adkins, J., Asami, R., Boer, W., … You, C.-F. (2013).
538 Interlaboratory study for coral Sr/Ca and other element/Ca ratio measurements.
539 *Geochemistry, Geophysics, Geosystems*, *14*(9), 3730–3750.

https://doi.org/10.1002/ggge.20230

Holcomb, M., Cohen, A. L., Gabitov, R. I., & Hutter, J. L. (2009). Compositional and morphological features of aragonite precipitated experimentally from seawater and biogenically by corals. *Geochimica et Cosmochimica Acta*, *73*(14), 4166–4179.

Holcomb, M., Venn, A. A., Tambutté, E., Tambutté, S., Allemand, D., Trotter, J., & McCulloch, M. (2014). Coral calcifying fluid pH dictates response to ocean acidification. *Scientific Reports*, *4*.

Hönisch, B., Ridgwell, A., Schmidt, D. N., Thomas, E., Gibbs, S. J., Sluijs, A., … Greene, S. E. (2012). The geological record of ocean acidification. *Science*, *335*(6072), 1058–1063. https://doi.org/10.1126/science.1208277

Hori, M., Shirai, K., Kimoto, K., Kurasawa, A., Takagi, H., Ishida, A., … Sano, Y. (2018). Chamber formation and trace element distribution in the calcite walls of laboratory cultured planktonic foraminifera (Globigerina bulloides and Globigerinoides ruber). *Marine Micropaleontology*, *140*, 46–55. https://doi.org/10.1016/J.MARMICRO.2017.12.004

Jacob, D. E., Wirth, R., Agbaje, O. B. A., Branson, O., & Eggins, S. M. (2017). Planktic foraminifera form their shells via metastable carbonate phases. *Nature Communications*, *8*(1), 1265. https://doi.org/10.1038/s41467-017-00955-0

Jolivet, A., Bardeau, J.-F., Fablet, R., Paulet, Y.-M., & de Pontual, H. (2008). Understanding otolith biomineralization processes: new insights into microscale spatial distribution of organic and mineral fractions from Raman microspectrometry. *Analytical and Bioanalytical Chemistry*, *392*(3), 551–560.

Jolivet, A., Bardeau, J.-F., Fablet, R., Paulet, Y.-M., & de Pontual, H. (2013). How do the organic and mineral fractions drive the opacity of fish otoliths? Insights using Raman microspectrometry. *Canadian Journal of Fisheries and Aquatic Sciences*, *70*(5), 711–

719. https://doi.org/10.1139/cjfas-2012-0298

Kamenos, N. A., Burdett, H. L., Aloisio, E., Findlay, H. S., Martin, S., Longbone, C., … Calosi, P. (2013). Coralline algal structure is more sensitive to rate, rather than the magnitude, of ocean acidification. *Global Change Biology*, *19*(12), 3621–3628.

Kamenos, N. A., Perna, G., Gambi, M. C., Micheli, F., & Kroeker, K. J. (2016). Coralline algae in a naturally acidified ecosystem persist by maintaining control of skeletal mineralogy and size. *Proceedings of the Royal Society of London B: Biological Sciences*, *283*(1840).

Knoll, A. H. (2003). Biomineralization and Evolutionary History. *Reviews in Mineralogy and Geochemistry*, *54*(1), 329–356. https://doi.org/10.2113/0540329

Mass, T., Giuffre, A. J., Sun, C.-Y., Stifler, C. A., Frazier, M. J., Neder, M., … Gilbert, P. U. P. A. (2017). Amorphous calcium carbonate particles form coral skeletons. *Proceedings of the National Academy of Sciences of the United States of America*, 201707890. https://doi.org/10.1073/pnas.1707890114

McCoy, S. J., & Kamenos, N. A. (2018). Coralline algal skeletal mineralogy affects grazer impacts. *Global Change Biology*. https://doi.org/10.1111/gcb.14370

McCulloch, M. T., D'Olivo Cordero, J. P., Falter, J., Holcomb, M., & Trotter, J. A. (2017). Coral calcification in a changing World: the interactive dynamics of pH and DIC up-regulation. *Nature Communications*, *8*, 15686.

Meibom, A., Cuif, J. P., Hillion, F., Constantz, B. R., Juillet-Leclerc, A., Dauphin, Y., … Dunbar, R. B. (2004). Distribution of magnesium in coral skeleton. *Geophysical Research Letters*, *31*(23), L23306.

Melancon, S., Fryer, B. J., Gagnon, J. E., & Ludsin, S. A. (2008). Mineralogical approaches to the study of biomineralization in fish otoliths. *Mineralogical Magazine*, *72*(2), 627–637. https://doi.org/10.1180/minmag.2008.072.2.627

590 Morse, J. W., Mucci, A., & Millero, F. J. (1980). The solubility of calcite and aragonite in
591 seawater of 35%. salinity at 25°C and atmospheric pressure. *Geochimica et*
592 *Cosmochimica Acta*, *44*(1), 85–94. https://doi.org/10.1016/0016-7037(80)90178-7
593 Nasdala, L., Wenzel, M., Vavra, G., Irmer, G., Wenzel, T., & Kober, B. (2001).
594 Metamictisation of natural zircon: accumulation versus thermal annealing of
595 radioactivity-induced damage. *Contributions to Mineralogy and Petrology*, *141*(2), 125–
596 144. https://doi.org/10.1007/s004100000235
597 Nash, M. C., Opdyke, B. N., Troitzsch, U., Russell, B. D., Adey, W. H., Kato, A., … Kline,
598 D. I. (2013). Dolomite-rich coralline algae in reefs resist dissolution in acidified
599 conditions. *Nature Climate Change*, *3*(3), 268–272.
600 https://doi.org/10.1038/nclimate1760
601 Nash, M. C., Troitzsch, U., Opdyke, B. N., Trafford, J. M., Russell, B. D., & Kline, D. I.
602 (2011). First discovery of dolomite and magnesite in living coralline algae and its
603 geobiological implications. *Biogeosciences*, *8*(11), 3331–3340.
604 https://doi.org/10.5194/bg-8-3331-2011
605 Nehrke, G., Nouet, J., & Treude, T. (2011). Confocal Raman microscope mapping as a tool
606 to describe different mineral and organic phases at high spatial resolution within marine
607 biogenic carbonates: case study on Nerita undata (Gastropoda, Neritopsina).
608 *Biogeosciences*, *8*, 3761–3769.
609 Perrin, J., Vielzeuf, D., Laporte, D., Ricolleau, A., Rossman, G. R., & Floquet, N. (2016).
610 Raman characterization of synthetic magnesian calcites. *American Mineralogist*,
611 *101*(11), 2525–2538.
612 Ridgwell, A., & Schmidt, D. N. (2010). Past constraints on the vulnerability of marine
613 calcifiers to massive carbon dioxide release. *Nature Geoscience*, *3*(3), 196–200.
614 Ries, J. B. (2011). A physicochemical framework for interpreting the biological calcification

615 response to CO2-induced ocean acidification. *Geochimica et Cosmochimica Acta*,
616 *75*(14), 4053–4064.
617 Risk, M. J., Heikoop, J. M., Snow, M. G., & Beukens, R. (2002). Lifespans and growth
618 patterns of two deep-sea corals: Primnoa resedaeformis and Desmophyllum cristagalli.
619 *Hydrobiologia*, *471*(1/3), 125–131. https://doi.org/10.1023/A:1016557405185
620 Roger, L. M., George, A. D., Shaw, J., Hart, R. D., Roberts, M., Becker, T., … Evans, N. J.
621 (2017). Geochemical and microstructural characterisation of two species of cool-water
622 bivalves (Fulvia tenuicostata and Soletellina biradiata) from Western Australia.
623 *Biogeosciences*, *14*(6), 1721–1737. https://doi.org/10.5194/bg-14-1721-2017
624 Ross, C. L., Falter, J. L., Schoepf, V., & McCulloch, M. T. (2015). Perennial growth of
625 hermatypic corals at Rottnest Island, Western Australia (32°S). *PeerJ*, *3*, e781.
626 https://doi.org/10.7717/peerj.781
627 Ross, C. L., Schoepf, V., DeCarlo, T. M., & McCulloch, M. T. (2018). Mechanisms and
628 seasonal drivers of calcification in the temperate coral Turbinaria reniformis at its
629 latitudinal limits. *Proceedings of the Royal Society B: Biological Sciences*, *285*(1879),
630 20180215. https://doi.org/10.1098/rspb.2018.0215
631 Schoepf, V., Jury, C. P., Toonen, R. J., & McCulloch, M. T. (2017). Coral calcification
632 mechanisms facilitate adaptive responses to ocean acidification. *Proceedings. Biological*
633 *Sciences*, *284*(1868), 20172117. https://doi.org/10.1098/rspb.2017.2117
634 Shapiro, O. H., Kramarsky-Winter, E., Gavish, A. R., Stocker, R., & Vardi, A. (2016). A
635 coral-on-a-chip microfluidic platform enabling live-imaging microscopy of reef-building
636 corals. *Nature Communications*, *7*, 10860. https://doi.org/10.1038/ncomms10860
637 Smith, A. M., Sutherland, J. E., Kregting, L., Farr, T. J., & Winter, D. J. (2012).
638 Phylomineralogy of the Coralline red algae: Correlation of skeletal mineralogy with
639 molecular phylogeny. *Phytochemistry*, *81*, 97–108.

https://doi.org/10.1016/J.PHYTOCHEM.2012.06.003

Smith, E., & Dent, G. (2005). *Modern Raman spectroscopy: a practical approach*. West Sussex, England: John Wiley & Sons.

Spero, H. J., Eggins, S. M., Russell, A. D., Vetter, L., Kilburn, M. R., & Hönisch, B. (2015). Timing and mechanism for intratest Mg/Ca variability in a living planktic foraminifer. *Earth and Planetary Science Letters*, *409*, 32–42. https://doi.org/10.1016/J.EPSL.2014.10.030

Stolarski, J., Bosellini, F. R., Wallace, C. C., Gothmann, A. M., Mazur, M., Domart-Coulon, I., … Meibom, A. (2016). A unique coral biomineralization pattern has resisted 40 million years of major ocean chemistry change. *Scientific Reports*, *6*, 27579. https://doi.org/10.1038/srep27579

Sturgeon, R. E., Willie, S. N., Yang, L., Greenberg, R., Spatz, R. O., Chen, Z., … Thorrold, S. (2005). Certification of a fish otolith reference material in support of quality assurance for trace element analysis. *Journal of Analytical Atomic Spectrometry*, *20*(10), 1067–1071. https://doi.org/10.1039/B503655K

Thillainath, E. C., McIlwain, J. L., Wilson, S. K., & Depczynski, M. (2016). Estimating the role of three mesopredatory fishes in coral reef food webs at Ningaloo Reef, Western Australia. *Coral Reefs*, *35*(1), 261–269. https://doi.org/10.1007/s00338-015-1367-y

Trotter, J. A., Pattiaratchi, C., Montagna, P., Taviani, M., Falter, J., Thresher, R., … McCulloch, M. T. (2018). Unveiling the Perth Canyon and its deep-water faunas. *Biogeosciences Discussions*, 1–35. https://doi.org/10.5194/bg-2018-319

Tyrrell, T., & Zeebe, R. E. (2004). History of carbonate ion concentration over the last 100 million years. *Geochimica et Cosmochimica Acta*, *68*(17), 3521–3530.

Venn, A., Tambutte, E., Holcomb, M., Allemand, D., & Tambutte, S. (2011). Live tissue imaging shows reef corals elevate pH under their calcifying tissue relative to seawater.

665 *PLoS One*, *6*(5), e20013. https://doi.org/10.1371/journal.pone.0020013
666 Veron, J. E. N. (2008). Mass extinctions and ocean acidification: biological constraints on
667 geological dilemmas. *Coral Reefs*, *27*(3), 459–472.
668 Von Euw, S., Zhang, Q., Manichev, V., Murali, N., Gross, J., Feldman, L. C., … Falkowski,
669 P. G. (2017). Biological control of aragonite formation in stony corals. *Science*,
670 *356*(6341), 933–938.
671 Wall, M., & Nehrke, G. (2012). Reconstructing skeletal fiber arrangement and growth mode
672 in the coral Porites lutea (Cnidaria, Scleractinia): a confocal Raman microscopy study.
673 *Biogeosciences*, *9*(11), 4885–4895.
674 Wall, M., Ragazzola, F., Foster, L. C., Form, A., & Schmidt, D. N. (2015). pH up-regulation
675 as a potential mechanism for the cold-water coral Lophelia pertusa to sustain growth in
676 aragonite undersaturated conditions. *Biogeosciences*, *12*(23), 6869–6880.
677 https://doi.org/10.5194/bg-12-6869-2015
678 Wang, D., Hamm, L. M., Bodnar, R. J., & Dove, P. M. (2012). Raman spectroscopic
679 characterization of the magnesium content in amorphous calcium carbonates. *Journal of*
680 *Raman Spectroscopy*, *43*(4), 543–548.
681 Wehrmeister, U., Soldati, A. L., Jacob, D. E., Häger, T., & Hofmeister, W. (2009). Raman
682 spectroscopy of synthetic, geological and biological vaterite: a Raman spectroscopic
683 study. *Journal of Raman Spectroscopy*, *41*(2), 193–201. https://doi.org/10.1002/jrs.2438
684 Yoshinaga, J., Nakama, A., Morita, M., & Edmonds, J. S. (2000). Fish otolith reference
685 material for quality assurance of chemical analyses. *Marine Chemistry*, *69*(1), 91–97.
686 https://doi.org/10.1016/S0304-4203(99)00098-5
687 Zeebe, R. E., Ridgwell, A., & Zachos, J. C. (2016). Anthropogenic carbon release rate
688 unprecedented during the past 66 million years. *Nature Geoscience*, *9*(4), 325–329.
689 https://doi.org/10.1038/ngeo2681